Supporting information: Model description

St Kolev[1,2], A Bogaerts[1]

[1]Research group PLASMANT, Department of Chemistry, University of Antwerp, Universiteitsplein 1, B-2610 Antwerp, Belgium

[2]Faculty of Physics, Sofia University, 5 James Bourchier Boulevard, 1164 Sofia, Bulgaria

E-mail: skolev@phys.uni-sofia.bg

E-mail: annemie.bogaerts@uantwerpen.be

1. Argon kinetics

The argon kinetics taken into account in this work is similar to [1]. The model considers the following species: e – electrons, Ar – Argon atoms, Ar^+ – Argon ions, Ar_2^+ – Argon molecular ions, Ar (4s) – all 4s levels considered as a single lumped excitation level, Ar (4p) – all 4p levels considered as a single lumped excitation level, and Ar_2^* – which includes $Ar_2(^1\Sigma_u^+)$ and $Ar_2(^3\Sigma_u^+)$ excited molecules. The different processes considered in both models are listed in tables 1 and 2, along with the corresponding references for the rate coefficients and cross sections.

2. Cartesian model

The two models consider a slightly different set of equations, which is related to their specific aim and geometry. The 2D axisymmetric model considers the particle balance equations, the electron energy balance equation and the gas thermal balance. The 2D Cartesian model, on the other hand, considers the particle balance equations, the electron energy balance, the gas thermal balance and the Navier-Stokes equations for the gas flow description. In the following text we describe the equations used in the Cartesian model, as well as the boundary condition.

2.1. Particle balance equations

We use the drift-diffusion approximation and we solve the well-known particle balance equation:

$$\frac{\partial n_s}{\partial t} + \nabla \cdot \boldsymbol{G}_{\mathrm{s}} + (\boldsymbol{u}_{\mathrm{g}} \cdot \nabla) n_s = S_{\mathrm{c}}, \tag{1}$$

where n_s is the species density, $\boldsymbol{G}_{\mathrm{s}}$ is the species flux, $\boldsymbol{u}_{\mathrm{g}}$ is the gas velocity and S_c is the collision term representing the net number of particles produced or lost in the volume reactions included in tables 1 and 2. The index "s" represents all the species considered,

Table 1. Electron collisions included in the model.

Reaction	Rate coefficient	Reference
(R1) $e + Ar \rightarrow e + Ar$	BS[a]	[2]
(R2) $e + Ar \rightarrow e + Ar(4s)$	BS	[2]
(R3) $e + Ar \rightarrow e + Ar(4p)$	BS	[2]
(R4)[b] $e + Ar \rightarrow e + Ar(4d)$	BS	[2]
(R5) $e + Ar \rightarrow 2e + Ar^+$	BS	[2]
(R6) $e + Ar(4s) \rightarrow e + Ar(4p)$	BS	[3]
(R7) $e + Ar(4s) \rightarrow 2e + Ar^+$	BS	[4]
(R8) $e + Ar(4p) \rightarrow 2e + Ar^+$	BS	[4]
(R9) $e + Ar(4s) \rightarrow e + Ar$	BS, DB[c]	[2]
(R10) $e + Ar(4p) \rightarrow e + Ar$	BS, DB	[2]
(R11) $e + Ar(4p) \rightarrow e + Ar(4s)$	BS, DB	[3]
(R12) $Ar^+ + 2e \rightarrow Ar + e$	$k_{(m^6/s)} = 8.75 \times 10^{-39} T_e^{-4.5}(eV)$	[5]
(R13) $Ar^+ + e + Ar \rightarrow Ar + Ar$	$k_{(m^6/s)} = 1.5 \times 10^{-40} (T_g(K)/300)^{-2.5}$	[6]
(R14) $Ar_2^+ + e \rightarrow Ar^+ + Ar + e$	$k_{(m^3/s)} = 1.11 \times 10^{-12} \exp\left(-\frac{2.94-3(Tg(eV)-0.026)}{Te(eV)}\right)$	[7]
(R15) $Ar_2^+ + e \rightarrow Ar + Ar(4s)$	$k_{(m^3/s)} = 1.04 \times 10^{-12} [300/T_e(K)]^{0.67} \frac{1-\exp[-418/Tg(K)]}{1-0.31\exp[-418/Tg(K)]}$	[8,9]
(R16) $Ar_2^* + e \rightarrow Ar_2^+ + 2e$	$k_{(m^3/s)} = 9 \times 10^{-14} [T_e(eV)]^{0.7} \exp[-3.66/T_e(eV)]$	[10]
(R17) $Ar_2^* + e \rightarrow 2Ar + e$	$k_{(m^3/s)} = 1 \times 10^{-15}$	[10]

[a] Boltzmann solver: The rate coefficients are calculated from the corresponding cross sections, based on the solution of the Boltzmann equation with BOLSIG+ [11].

[b] This process is included only as an energy loss channel without considering the conservation equation for Ar(4d)

[c] Detailed balance: The rate coefficients for the superelastic processes are calculated using the detailed balance principle [12] incorporated in BOLSIG+ [11].

Table 2. Heavy species collisions and radiative transitions included in the model.

Reaction	Rate coefficient/collision frequency	Reference
(R18) $Ar(4s) + Ar(4s) \rightarrow Ar_2^+ + e$	$k_{(m^3/s)} = \frac{1}{2} 6.3 \times 10^{-16} (T_g(K)/300)^{-1/2}$	[13]
(R19) $Ar(4s) + Ar(4s) \rightarrow Ar^+ + Ar + e$	$k_{(m^3/s)} = 1.62 \times 10^{-16} (T_g(K))^{1/2}$	[14]
(R20) $Ar(4s) + Ar(4p) \rightarrow Ar^+ + Ar + e$	$k_{(m^3/s)} = 1.62 \times 10^{-16} (T_g(K))^{1/2}$	[14]
(R21) $Ar(4p) + Ar(4p) \rightarrow Ar^+ + Ar + e$	$k_{(m^3/s)} = 1.62 \times 10^{-16} (T_g(K))^{1/2}$	[14]
(R22) $Ar(4p) + Ar \rightarrow Ar(4s) + Ar$	$k_{(m^3/s)} = 5 \times 10^{-18}$	[15]
(R23) $Ar^+ + 2Ar \rightarrow Ar_2^+ + Ar$	$k_{(m^6/s)} = 2.5 \times 10^{-43} (T_g(K)/300)^{-3/2}$	[15]
(R24) $Ar_2^+ + Ar \rightarrow Ar^+ + 2Ar$	$k_{(m^3/s)} = \frac{6.06 \times 10^{-12}}{Tg(K)} \exp\left(-\frac{1.51 \times 10^4}{Tg(K)}\right)$	[7]
(R25) $Ar(4s) + 2Ar \rightarrow Ar_2^* + Ar$	$k_{(m^6/s)} = 3.3 \times 10^{-44}$	[10]
(R26) $Ar(4p) + 2Ar \rightarrow Ar_2^* + Ar$	$k_{(m^6/s)} = 2.5 \times 10^{-44}$	[15]
(R27) $Ar_2^* + Ar_2^* \rightarrow Ar_2^+ + 2Ar + e$	$k_{(m^3/s)} = 5 \times 10^{-16} (T_g(K)/300)^{1/2}$	[15]
(R28) $Ar_2^* + Ar(4s) \rightarrow Ar_2^+ + Ar + e$	$k_{(m^3/s)} = 6 \times 10^{-16} (T_g(K)/300)^{1/2}$	[15]
(R29) $Ar(4s) \rightarrow Ar + h\nu$	$\nu_{c(s^{-1})} = g_{eff}^a \times 3.145 \times 10^8$	[14]
(R30) $Ar(4p) \rightarrow Ar(4s) + h\nu$	$\nu_{c(s^{-1})} = 4.4 \times 10^7$	[14]
(R31) $Ar_2^* \rightarrow 2Ar + h\nu$	$\nu_{c(s^{-1})} = 6 \times 10^7$	[10]

[a] $g_{eff} = (1.15/\pi)\sqrt{(\lambda_{4s}/(6H))}$, where $\lambda_{4s} = 105.7$ nm and H is a characteristic dimension of the reactor, i.e., taken as $H = 3$ mm in our case.

except for the argon atoms, i.e. e, Ar^+, Ar_2^+, Ar (4s), Ar (4p), Ar_2^*. The argon gas atom density is considered to be constant.

The flux of the different species is expressed in the following way: the electron flux is

$$\boldsymbol{G}_{\mathrm{e}} = -D_e \nabla (n_e) + \frac{q_e}{|q_e|} \mu_e n_e \boldsymbol{E}, \tag{2}$$

the ion flux is

$$\boldsymbol{G}_{\mathrm{s}} = -D_s \nabla (n_s) + \frac{q_s}{|q_s|} \mu_s n_s \boldsymbol{E} \tag{3}$$

and for the neutral species (Ar (4s),Ar (4p) and Ar_2^*) the flux is only determined by diffusion: $\boldsymbol{G}_{\mathrm{s}} = -D_s \nabla (n_s)$. In the above expressions, D is the diffusion coefficient and, μ is the mobility of the corresponding species, $\boldsymbol{E}$ is the electric field vector and q_s is the charge of the given species type.

The transport coefficients used in the models are as follows: μ_e is derived from BOLSIG+ and the Ar^+ mobility is defined as in [16]:

$$\mu_{Ar^+} = \frac{1.01 \times 10^5}{p_{\mathrm{g}}(\mathrm{Pa})} \frac{T_g(K)}{273.16} 1.52 \times 10^{-4} \left(\mathrm{m^2 V^{-1} s^{-1}}\right), \tag{4}$$

where p_{g} is the gas pressure and T_{g} is the gas temperature. The latter expression is also used for the molecular ion mobility with a certain correction factor [16], i.e. $\mu_{Ar_2^+} = 1.2 \times \mu_{Ar^+}$. The electron and ion diffusion coefficients are derived from their corresponding mobilities based on the Einstein relation. The Ar (4s) diffusion coefficient is defined according to [17] as

$$D_{\mathrm{Ar(4s)}} = (1/n_{\mathrm{Ar}}) 1.16 \times 10^{20} (T_{\mathrm{Ar(4s)}}(K)/300)^{1/2} \quad (\mathrm{m^2/s}), \tag{5}$$

For the diffusion coefficients of Ar (4p) and Ar_2^*, due to the lack of literature data, we assume the same expression as for Ar (4s). This might look as a very rough approximation especially for Ar_2^*, but it does not significantly affect the final results because the diffusion terms in the balance equations for Ar (4p) and Ar_2^* remain negligible compared to the reaction terms. We also assume that the temperature of all heavy species is equal to the gas temperature (T_{g}).

2.2. Averaged electron energy balance

The averaged electron energy is found by solving

$$\frac{\partial n_e \overline{\varepsilon}_e}{\partial t} + \nabla . \boldsymbol{G}_{\varepsilon,\mathrm{e}} + (\boldsymbol{u}_{\mathrm{g}} \cdot \nabla) n_e \overline{\varepsilon}_e = q_e \boldsymbol{E} . \boldsymbol{G}_{\mathrm{e}} + n_e \triangle \overline{\varepsilon}_e + Q_{\mathrm{bg}}, \tag{6}$$

where the electron energy flux is expressed as $\boldsymbol{G}_{\varepsilon,\mathrm{e}} = -D_{\varepsilon,e} \nabla (n_e \overline{\varepsilon}_e) - \mu_{\varepsilon,e} n_e \overline{\varepsilon}_e \boldsymbol{E}$. Here we use the following notations: $\overline{\varepsilon}_e$ is the electron averaged energy (averaged over the energy distribution function), $D_{\varepsilon,e}$ is the electron energy diffusion coefficient, $\mu_{\varepsilon,e}$ is the electron energy mobility and $\triangle \overline{\varepsilon}_e$ represents the averaged electron energy losses in the different collision events. $D_{\varepsilon,e}$ and $\mu_{\varepsilon,e}$ are derived from the electron mobility: $\mu_{\varepsilon,e} = (5/3)\mu_e$ and $D_{\varepsilon,e} = (2/3)\mu_{\varepsilon,e} \overline{\varepsilon}_e$. In order to make the numerical calculations more

stable, we add a constant background power density Q_{bg} everywhere in the simulated domain (i.e. the plasma and the neutral gas). In this way, in the whole domain we artificially sustain a low density plasma ($n_{\mathrm{e}} < 1 \times 10^{16}$ m^{-3}) with a certain temperature derived self-consistently (around 1.8 eV in the bulk). This power density is low enough so that it does not affect the arc behaviour, which is verified by several simulations with different background power Q_{bg}. The presence of background plasma allows us to significantly reduce the gradients in the variables between the arc and the background and thus to reduce the requirements to the discretization grid. The electron density due to this artificial heating is at least 4 orders of magnitude lower than the arc electron density.

2.3. Poisson equation

The electric field in the discharge is calculated with the Poisson equation:

$$\triangle\Phi = -\rho_{\mathrm{q}}/\varepsilon_0, \tag{7}$$

where Φ is the electric potential, ρ_{q} is the charge density and ε_0 is the vacuum dielectric permittivity.

2.4. Gas flow equations

For a proper description of the gliding arc we need to describe the gas flow which is responsible for the arc displacement. In the experiment considered here [18] the gas is supplied with a small nozzle positioned close to the shortest electrode distance position. With the 2D Cartesian model we are not able to accurately describe the gas flow from the nozzle. Therefore we solve here only a simplified version of the Navier-Stokes equations by adjusting the inlet boundary velocity in order to obtain a gas velocity similar to what is observed in the experiments. A rough estimation of the experimental gas velocity is obtained by examination of the arc displacement shown on successive high-speed photographs [18]. Note that this is, however, not a very accurate method since it is well possible that the arc does not have exactly the same velocity as the gas but slightly lower values [19, 20]. Note that measurements in [20] show that the gas-to-arc velocity ratio is in the order of 1.2-1.3. The equations solved are the incompressible Navier-Stokes equations for a Newtonian fluid excluding the inertial term, i.e. in the regime of Stokes flow:

$$\rho_{\mathrm{g}}\frac{\partial \boldsymbol{u}_{\mathrm{g}}}{\partial t} = \nabla.(-p_{\mathrm{g}}\boldsymbol{I} + \mu_{\mathrm{g}}(\nabla\boldsymbol{u}_{\mathrm{g}} + (\nabla\boldsymbol{u}_{\mathrm{g}})^{\mathrm{T}})), \tag{8}$$

$$\rho_{\mathrm{g}}\nabla.\boldsymbol{u}_{\mathrm{g}} = 0, \tag{9}$$

where ρ_{g} is the gas density, p_{g} is the gas pressure, μ_{g} is the gas viscosity, $\boldsymbol{I}$ is the unit matrix and the superscript T stands for the tensor transpose operation. In the model, the Navier-Stokes equations are not solved together with the other equations, because this would yield excessive calculations times, but instead they are solved first separately and then the obtained velocity distribution is used as input data.

2.5. Gas thermal balance

Here we calculate the gas temperature by solving the gas thermal balance

$$\rho_{\mathrm{g}} C_p \frac{\partial T_{\mathrm{g}}}{\partial t} + \rho_{\mathrm{g}} C_p \boldsymbol{u}_{\mathrm{g}} . \nabla T_{\mathrm{g}} - \nabla . \left(k_{\mathrm{g}} \nabla T_{\mathrm{g}} \right) = Q_{\mathrm{g}}, \tag{10}$$

where C_p is the gas heat capacity of Ar, k_{g} is the Ar thermal conductivity and Q_{g} is a heat source, which in our case results from the plasma heating. This includes all the energy lost by the electrons in elastic and inelastic collisions, which is assumed to be finally transferred to the gas, as well as the energy transferred from the ions to the gas. The ions gain energy from the electric field. The total gas heat source is thus expressed as:

$$Q_{\mathrm{g}} = \frac{3 m_e m_{Ar}}{\left(m_e + m_{Ar} \right)^2} n_e n_{Ar} k_1 e \left(T_e - T_{\mathrm{g}} \right) + \sum_i \triangle \varepsilon_i k_i n_e n_{i-t} + \boldsymbol{j}_{ion} \cdot \boldsymbol{E}, \tag{11}$$

where the first term represents the electron energy losses due to elastic collisions with rate coefficient k_1, the second term represents the sum of all electron energy losses due to inelastic collisions with energy loss $\triangle \varepsilon_i$, rate coefficient k_i and collision target density n_{i-t} for the i-th process, and the third term is the ion heating being the scalar product of the total ion current density $\boldsymbol{j}_{\mathrm{ion}}$ and the electric field $\boldsymbol{E}$. In the above expression the electron and gas temperatures are expressed in "eV". Here we neglect the energy loss due to radiation from excited atoms which is estimated to be relatively small (see also the comments in [5], page 277). The major term in equation (7) is usually the elastic energy transfer and only in the cathode layer the second and third terms in the right-hand side become considerable. The reason for the latter is the higher electron temperature in this region, enhancing the excitation processes, as well as the strong electric field which increases the ion velocity and the $(\boldsymbol{j}_{\mathrm{ion}} \cdot \boldsymbol{E})$ term.

In summary, the 2D Cartesian model includes equations (1), (6)-(10).

2.6. Boundary conditions

The boundary conditions (BC) are summarized in table 3 and some further explanation is given below.

The boundary condition for the electron balance equation (1) and the electron energy balance equation (6) at the cathode should include the electron emission processes in addition to the thermal flux. This yields the following BC for the normal electron flux at the cathode [21, 22]:

$$\boldsymbol{n} \cdot \boldsymbol{G}_{\mathrm{e}} = \frac{1}{2} \mathrm{v}_{\mathrm{e,th}} n_{\mathrm{e}} - \left[\sum_s \gamma_s \left(\boldsymbol{G}_s \cdot \boldsymbol{n} \right) + \boldsymbol{G}_{\mathrm{TF}} \cdot \boldsymbol{n} \right] \tag{12}$$

and for the normal electron energy flux [22]

$$\boldsymbol{n} \cdot \boldsymbol{G}_{\varepsilon,\mathrm{e}} = \frac{5}{6} \mathrm{v}_{\mathrm{e,th}} n_{\mathrm{e}} \overline{\varepsilon}_e - \left[\sum_s \gamma_s \varepsilon_{s,\mathrm{sec}} \left(\boldsymbol{G}_s \cdot \boldsymbol{n} \right) + \varepsilon_{\mathrm{TF}} \boldsymbol{G}_{\mathrm{TF}} \cdot \boldsymbol{n} \right] \tag{13}$$

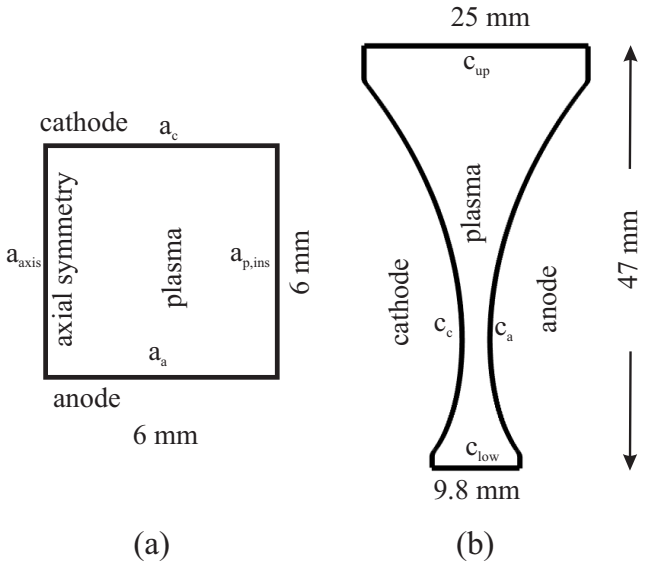

Figure 1. Geometries considered in the models:

(a) 2D axisymmetric model geometry with the following boundaries: a_c - cathode-plasma interface, a_a - anode, a_{axis} - axial symmetry axis, $a_{c,ins}$ - insulation boundary, $a_{p,ins}$ - insulation boundary for the plasma (zero fluxes).

(b) 2D Cartesian model geometry with the following boundaries: c_c - cathode, c_a - anode, c_{low} - upstream boundary used as a gas inlet, c_{up} - upper (downstream) boundary providing gas outflow.

In the above expressions $v_{e,th} = \sqrt{\frac{8k_BT_e}{\pi m_e}}$ is the electron thermal velocity, γ_s is the secondary electron emission coefficient due to ion impact for the two types of ions (Ar^+ and Ar_2^+) having a normal flux $\boldsymbol{G}_s$ towards the cathode. Hence, the sum is taken over these two types of ions. k_B is the Boltzmann constant, m_e is the electron mass, $\varepsilon_{s,sec}$ is the averaged energy of the secondary electrons and ε_{TF} is the averaged energy of the emitted electrons due to thermo-field emission. The value of γ_s is not known and it is very dependent on the cathode material and surface properties. $\boldsymbol{G}_{TF}$ is the electron flux due to thermo-field emission. It is known [23] that the combined effect of the thermal and field electron emissions (also denoted as thermo-field (TF) emission) is much stronger compared to the sum of both independent processes. Therefore, we use here the expression for the electron emission current density, which accounts for their combined effect [23]. It is also important to note that in the calculation of the field emission usually not the real normal electric field (E_n) is considered but an effective field which is calculated as $E_{n,eff} = \text{FEF} * E_n$. The factor FEF is called "Field enhancement factor" and accounts for the effective enhancement of the field due to surface roughness and sharp protrusions [23]. Similarly to γ_s, this factor will be very dependent on a particular experiment and it may even change during the experiments because of surface modification as a results of the arc impact.

For the non-emitting walls (anode and c_{up}) the BC includes only the thermal

electron flux:

$$\boldsymbol{n} \cdot \boldsymbol{G}_{\mathrm{e,n}} = \frac{1}{2} \mathrm{v}_{\mathrm{e,th}} n_{\mathrm{e}} \tag{14}$$

The electron energy flux in this case is then:

$$\boldsymbol{n} \cdot \boldsymbol{G}_{\varepsilon,\mathrm{e}} = \frac{5}{6} \mathrm{v}_{\mathrm{e,th}} n_{\mathrm{e}} \overline{\varepsilon}_e. \tag{15}$$

The ion flux at the walls, for both the Ar^+ and Ar_2^+ ions, is found by accounting for their thermal velocity and their drift velocity due to the electric field:

$$\boldsymbol{n} \cdot \boldsymbol{G}_s = \frac{1}{4} \mathrm{v}_{s,\mathrm{th}} n_s + \max\left(\frac{q_s}{|q_s|} \mu_s n_s \boldsymbol{E} \cdot \boldsymbol{n}, 0 \right) \tag{16}$$

where the function "max" returns the maximum of both arguments. In this case it sets the drift flux $\frac{q_s}{|q_s|} \mu_s n_s \boldsymbol{E} \cdot \boldsymbol{n}$ to 0 if it becomes negative, i.e. if the flux is directed towards the plasma domain. The neutral species, i.e. Ar(4s), Ar(4p) and Ar_2^*, are supposed to reach the wall due to thermal motion only and thus their BC on the wall is:

$$\boldsymbol{n} \cdot \boldsymbol{G}_s = \frac{1}{4} \mathrm{v}_{s,\mathrm{th}} n_s \tag{17}$$

where $s = \mathrm{Ar(4s)}, \mathrm{Ar(4p)}, \mathrm{Ar}_2^*$.

All these boundary conditions, as well as the other (more simple) boundary conditions, are summarised in tables 3 and 4.

Table 3. Boundary conditions used in the 2D Cartesian model, at the various boundaries (see figure 1); see text for the equation numbers. V_{c} is the cathode potential with respect to the grounded anode.

eq.	(1)	(1)	(1)	(6)	(7)	(8),(9)	(10)
variable	n_{e}	n_{Ar^+} $n_{\mathrm{Ar}_2^+}$	$n_{\mathrm{Ar(4s)}}$ $n_{\mathrm{Ar(4p)}}$ $n_{\mathrm{Ar}_2^+}$	$\overline{\varepsilon}_e$	Φ	$\boldsymbol{u}_{\mathrm{g}}$ p_{g}	T_{g}
c_c	(12)	(16)	(17)	(13)	$\Phi = V_{\mathrm{c}}$	$\boldsymbol{u}_{\mathrm{g}} = 0$	$T_{\mathrm{g}} = 293$ K
c_a	(14)	(16)	(17)	(15)	$\Phi = 0$	$\boldsymbol{u}_{\mathrm{g}} = 0$	$T_{\mathrm{g}} = 293$ K
$\mathrm{c}_{\mathrm{low}}$	$\boldsymbol{n} \cdot \alpha = 0$; $\alpha = \boldsymbol{G}_{\mathrm{s}}$, $\boldsymbol{G}_{\varepsilon,\mathrm{e}}$, $\nabla\Phi$					$\boldsymbol{n} \cdot \boldsymbol{u}_{\mathrm{g}} = 3$ m/s	$T_{\mathrm{g}} = 293$ K
c_{up}	(14)	$\boldsymbol{n} \cdot \nabla n_s = 0$		(15)	$\Phi = 0$	$p = 101$ kPa	$\boldsymbol{n} \cdot \nabla T_{\mathrm{g}} = 0$

Finally, we specify certain conditions for the external circuit and the power supply. In both models (Cartesian and Axisymmetric), the external circuit is represented by a fixed voltage source $V_{\mathrm{source}} = 3700$ V and serially connected resistor R_{b}.

3. Axisymmetric model

The axisymmetric plasma model used here is based on equations (1), (6), (7) and (10), i.e. the same set of equations as the Cartesian model, the gas flow which is excluded ($\boldsymbol{u}_\mathrm{g} = 0$). As explained in the manuscript, the gas flow effect is replaced here by the addition of an effective loss terms in all balance equations (i.e. all except in the Poisson equation). The aim of the additional loss terms is to effectively account for the stretching of the gliding discharge as a result of the gas flow and thus to account for the convective processes. The loss terms is introduced on the right hand side of equations 1, 6 and 10. These terms are introduced as effective loss processes with a constant frequency ν_elong, equal for all equations. Thus the loss terms will be proportional to $-\alpha\nu_\mathrm{elong}$, where α represents the conserved variable i.e. $\alpha = n_\mathrm{e}$, n_{Ar^+}, $n_{\mathrm{Ar}_2^+}$, $n_{\mathrm{Ar(4s)}}$, $n_{\mathrm{Ar(4p)}}$, $n_{\mathrm{Ar}_2^*}$, $n_\mathrm{e}\overline{\varepsilon}_\mathrm{e}$, $\rho_\mathrm{g}C_pT_\mathrm{g}$. ν_elong has a unit of frequency [1/s] but it is related to the elongation speed of the plasma channel. Below we give more details about the definition of ν_elong and its relation to the real convection process.

Let us consider an elementary domain with volume Ω and length l in the direction of elongation. As a result of the elongation with speed v_elong for time $\mathrm{d}t$, the plasma channel length will increase with $\mathrm{d}l = v_\mathrm{elong}\mathrm{d}t$ and the domain volume will increase with $\mathrm{d}\Omega = \mathrm{d}lS_\mathrm{tr}$, where S_tr is the transverse cross section of the plasma channel. If we take into account that for some variables there is a minimum (background) value (α_bg) different from zero (like for example the gas temperature $T_\mathrm{g} = 293$ K) we can express the variation (reduction) of the conserved variable α as the difference between the initial (α) and the value after elongation α_elong:

$$\mathrm{d}\alpha = \alpha_\mathrm{elong} - \alpha = \frac{\alpha\Omega + \alpha_\mathrm{bg}\mathrm{d}\Omega}{\Omega + \mathrm{d}\Omega} - \alpha = -\frac{(\alpha - \alpha_\mathrm{bg})\mathrm{d}\Omega}{\Omega + \mathrm{d}\Omega} \approx$$
$$-\frac{(\alpha - \alpha_\mathrm{bg})\mathrm{d}\Omega}{\Omega} = -(\alpha - \alpha_\mathrm{bg})\frac{\mathrm{d}l}{l} = -(\alpha - \alpha_\mathrm{bg})v_\mathrm{elong}\frac{\mathrm{d}t}{l} \tag{18}$$

Which is based on the fact that the variables are conserved i.e. $\alpha\Omega + \alpha_\mathrm{bg}\mathrm{d}\Omega = \alpha_\mathrm{elong}(\Omega + \mathrm{d}\Omega)$ and the fact that $\mathrm{d}\Omega \ll \Omega$. Thus for the effective loss term due to convection we obtain:

$$\frac{\mathrm{d}\alpha}{\mathrm{d}t} = -(\alpha - \alpha_\mathrm{bg})v_\mathrm{elong}/l = -(\alpha - \alpha_\mathrm{bg})\nu_\mathrm{elong} \tag{19}$$

The above approach allows us approximately to take into account the convection processes in the gliding discharge while representing the plasma channel by using a 2D axisymmetric model. In the model, we take α_bg to be zero for all variables except for the gas temperature: $T_\mathrm{g,bg} = 293$ K.

The geometry considered in this model is presented in figure 1(a). It is a simple rectangle with 6 mm distance between the electrodes.

References

[1] Kolev St and Bogaerts A 2015 2D model for a gliding arc discharge *Plasma Sources Sci. Technol.* **24** 015025

Table 4. Boundary conditions used in the 2D axisymmetric model, at the various boundaries (see figure 1); see text for the equation numbers.

eq.	(1)	(1)	(1)	(6)	(7)	(10)
variable	n_e	n_{Ar^+} $n_{\mathrm{Ar}_2^+}$	$n_{\mathrm{Ar(4s)}}$ $n_{\mathrm{Ar(4p)}}$ $n_{\mathrm{Ar}_2^+}$	$\overline{\varepsilon}_e$	Φ	T_g
$\mathrm{a_{p,ins}}$	$\boldsymbol{n}\cdot\alpha=0$; $\alpha=\boldsymbol{u}_\mathrm{g}$, $\boldsymbol{G}_\mathrm{s}$, $\boldsymbol{G}_{\varepsilon,\mathrm{e}}$, $\nabla\Phi$, ∇T_g					
a_c	(12)	(16)	(17)	(13)	$\Phi=V_c$	$T_\mathrm{g}=T_\mathrm{c}$
a_a	(14)	(16)	(17)	(15)	$\Phi=0$	$T_\mathrm{g}=293$ K
$\mathrm{a_{axis}}$	$\boldsymbol{n}\cdot\nabla\alpha=0$; $\alpha=n_\mathrm{s}$, $n_\mathrm{e}\overline{\varepsilon}_e$, Φ, T_g, T_c, Φ_cons					

[2] BIAGI-v7.1 database, www.lxcat.laplace.univ-tlse.fr; Transcribed from SF Biagi's Fortran code MAGBOLTZ, Version 7.1, 2004. http://consult.cern.ch/writeup/magboltz

[3] Bartschat K, Zeman V 1999 Electron-impact excitation from the (3p54s) metastable states of argon *Phys. Rev.* **A59** 2552

[4] Hyman H A 1979 Electron-impact ionization cross section for excited states of the rare gases (Ne, Ar, Kr, Xe), cadmium, and mercury *Phys. Rev. A* **20** 855-859

[5] Raizer Yu P, Gas Discharge Physics, (Berlin: Springer) p 62

[6] Dyatko N A, Ionikh Y Z, Kochetov I V, Marinov D L, Meshchanov A V, Napartovich A P, Petrov F B and Starostin S A 2008 Experiemntal and theoretical study of the transition between diffuse and contracted forms of the glow discharge in argon *J Phys* D: *Appl Phys* **41** 055204

[7] Jonkers J, van de Sande M, Sola A, Gamero A, Rodero A and van der Mullen J 2003 *Plasma Sources Sci. Technol.* **12** 464-474

[8] Cunningham A J, O'Malley T F and Hobson R M 1981 On the role of vibrational excitation in dissociative recombination *J. Phys.* B: *At. Mol. Phys.* **14** 773-782

[9] Castaños-Martinez E, Kabouzi Y, Makasheva K and Moisan M 2004 Modeling of microwave-sustained plasmas at atmospheric pressure with application to discharge contraction *Phys. Rev.* E **70** 066405

[10] Kannari F, Suda A, Obara M and Fujioka T 1983 Theoretical simulation of electron-beam-excited xenon-chloride (XeCl) Laser *IEEE J. Quant. Electron.* **19** 1587-1600

[11] Hagelaar G J M and Pitchford L C 2005 Solving the Boltzmann equation to obtain electron transport coefficients and the rate coefficients for fluid models *Plasma Sources Sci. Technol.* **14** 722-733

[12] Lieberman M A, Lichtenberg A J *Principles of Plasma Discharges and Materials Processing*, (Hoboken: John Wiley & Sons) 2005 p 267

[13] Bultel A, Ootegem B, Bourdon A and Vervisch P 2002 Influence of Ar_2^+ in argon collisional-radiative model *Phys. Rev.* E **65** 046406

[14] Gregório J, Leprince P, Boisse-Laporteand C and Alves L L 2012 Self-consistent modelling of atmospheric micro-plasmas produced by a microwave source *Plasma Sources Sci. Technol.* **21** 015013

[15] Lam S K, Zheng C-E, Lo D, Dem'yanov A and Napartovich A P 2000 Kinetics of Ar_2^* in high-pressure pure argon *J. Phys.* D: *Appl. Phys.* **33** 242-251

[16] Mcdaniel E W and Mason E A 1973 *The mobility and diffusion of ions in gases* (Wiley)

[17] Ferreira C M, Loureiro J and Ricard A 1985 Populations in the metastable and the resonance levels of the argon and stepwise ionization effects in a low-pressure argon positive column *J. Appl. Phys.* **57** 82-90

[18] Tu X, Gallon H J and Whitehead J C 2011 Electrical and optical diagnostics of atmospheric pressure argon gliding arc plasma jet, 30th ICPIG, August 28th September 2nd 2011, Belfast,

Northern Ireland, UK, C10

[19] Fridman A, Nester S, Kennedy L A Saveliev A and Mutaf-Yardemci O 1999 Gliding arc gas discharge *Progress in Energy and Combustion Science* **25** 211-231

[20] Richard F, Cormier J M, Pellerin S and Chapelle J 1996 Physical study of a gliding arc discharge *J. Appl. Phys.* **79** 22452250

[21] Hagelaar G J M, Fubiani G and Boeuf J-P 2011 Model of an inductively coupled negative ion source: I. General model description *Plasma Sources Sci. Technol.* **20** 015001

[22] Comsol Multiphysics 4.3a, Plasma module user's guide

[23] Jünter B, Puchkarev V F, Hantzsche E and Beilis I 1995 in *Hanbook of vacuum arc science and technology. Fundamentals and Applications* eds Boxman R, Sanders D M, Martin P M (Park Ridge, New Jersey: Noyes Publications) pp 158-174.